Conf-901007--47

JAN 1991

CONF-901007--47

DE91 006455

MHD CONSIDERATIONS FOR POLOIDAL-TOROIDAL COOLANT DUCTS OF SELF-COOLED BLANKETS

by

T. Q. Hua
Argonne National Laboratory
9700 South Cass Avenue
Argonne, IL 60439

and

J. S. Walker
Department of Mechanical and Industrial Engineering
University of Illinois
Urbana, IL 61801

For Presentation at the Ninth Topical Meeting
on the Technology of Fusion Energy,
October 7-11, 1990, Oak Brook, IL

DISCLAIMER

This report was prepared as an account of work sponsored by an agency of the United States Government. Neither the United States Government nor any agency thereof, nor any of their employees, makes any warranty, express or implied, or assumes any legal liability or responsibility for the accuracy, completeness, or usefulness of any information, apparatus, product, or process disclosed, or represents that its use would not infringe privately owned rights. Reference herein to any specific commercial product, process, or service by trade name, trademark, manufacturer, or otherwise does not necessarily constitute or imply its endorsement, recommendation, or favoring by the United States Government or any agency thereof. The views and opinions of authors expressed herein do not necessarily state or reflect those of the United States Government or any agency thereof.

The submitted manuscript has been authored by a contractor of the U. S. Government under contract No. W-31-109-ENG-38. Accordingly, the U. S. Government retains a nonexclusive, royalty-free license to publish or reproduce the published form of this contribution, or allow others to do so, for U. S. Government purposes.

MASTER

DISTRIBUTION OF THIS DOCUMENT IS UNLIMITED

MHD CONSIDERATIONS FOR POLOIDAL-TOROIDAL COOLANT DUCTS OF SELF-COOLED BLANKETS

T. Q. Hua, Argonne National Laboratory
9700 South Cass Avenue
Argonne, Illinois 60439
(708) 972-7753

J. S. Walker, University of Illinois
Department of Mechanical and Industrial Engineering
Urbana, Illinois 61801

Abstract

Magnetohydrodynamic flows of liquid metals through sharp elbow ducts with rectangular cross sections and with thin conducting walls in the presence of strong uniform magnetic fields are examined. The geometries simulate the poloidal-toroidal coolant channels in fusion tokamak blankets. Analysis for obtaining the three-dimensional numerical solutions are described. Results for pressure drop, velocity profiles and flow distribution are predicted for the upcoming joint ANL/KfK sharp elbow experiment. Results from a parametric study using fusion relevant parameters to investigate the three-dimensional pressure drop are presented for possible applications to blanket designs.

I. Introduction

In a liquid-metal-cooled blanket of a tokamak reactor, the pressure gradient in the liquid metal is proportional to the square of the magnetic field component which is perpendicular to the flow direction. This is because the motion of the liquid metal across the magnetic field induces electric currents in the fluid as well as in the electrically conducting coolant channel walls. The currents in the liquid metal interact with the magnetic field to produce an electromagnetic body force opposing the motion. In the presence of the large toroidal magnetic field, liquid metal flowing in the poloidal direction at the first wall could result in excessive material stresses and require large pumping power. If the flow direction is aligned parallel to the strong toroidal field, then the pressure gradient will be substantially reduced, by a factor of 100 for a typical toroidal to poloidal field ratio of 10 to 1. A blanket design with toroidal first wall coolant channels was first proposed in the Blanket Comparison and Selection Study [1] and more recently was adopted in the blanket design for NET [2]. In both designs, the flows to the first wall coolant channels are fed by poloidal ducts or a combination of poloidal and radial ducts. However, several issues were left unanswered, which may be critical to the feasibility and attractiveness of these designs, regarding flow distributions and the pressure drops associated with the turning of the flow from poloidal to toroidal.

In this paper, we examine the flow of a liquid metal through two conducting rectangular ducts which are beveled at one end and joined together to form a 90° miter corner. The uniform magnetic field is almost perpendicular to one duct, hereafter referred to as the poloidal duct, and almost parallel to the other duct, known as the toroidal duct. Figure 1 shows the two orientations of the magnetic field relative to the centerline axes of the ducts. The backward elbow (Fig. 1b) is obtained by rotating the magnetic field lines 90° clockwise in the forward elbow geometry (Fig. 1a). The flow paths and flow distributions through the region near the elbow are markedly different in these two geometries, but our results show that the flow is never stagnant in a large region near the bend nor in the toroidal duct as was previously predicted by Hunt and Holroyd [3].

The scheme of analysis presented in this paper is purely numerical in all regions of the flow, and the finite difference solutions are three dimensional. A hybrid analytical-numerical scheme had been developed to treat the forward elbow problem [4], and a particular backward elbow problem in which the field lines form a 45° angle with the ducts' centerline axes [5]. In the hybrid scheme, the duct is treated as three separate sectors; two of the three sectors are semi-infinite straight constant cross sectional area rectangular ducts which are joined together by a variable cross sectional area duct sector. Analytical solutions using eigenfunction expansions are obtained for the variables in the straight ducts, and finite difference numerical solutions are obtained for the variable area duct. These solutions are then matched at their common boundaries by minimizing the sum of the differences squared of the variables using the Galerkin technique. The hybrid scheme is very new for this type of problem and can be further enhanced and refined through comparison of the

solutions with those obtained by the numerical scheme as well as with experiments. The numerical scheme used in this paper has been previously applied to various duct geometries and successfully validated by experimental data gathered at the ALEX facility [6] over the past few years. The purely numerical scheme was developed for the elbow problems to allow more flexibility in specifying the physical and geometrical parameters in order to support the design of the upcoming experiments which will be conducted jointly by Argonne National Laboratory (ANL) and Kernforschungzentrum Karlsruhe (KfK), and to provide analytical support for the KfK blanket design for NET. Just as importantly, the availability of the numerical solutions has since resulted in improvement of the hybrid scheme.

II. Problem Formulation

A. Forward Elbow

Figure 1a shows a schematic of the elbow and the uniform planar magnetic field, $\underset{\sim}{B} = B_o\hat{y}$. The centerline axis of the toroidal duct forms an angle θ_3 with the x-axis, where $45° < \theta_3 < 90°$, and the angle between the poloidal duct and the x-axis is $\theta_1 = \theta_3 - 90°$, $-45° < \theta_1 < 0°$. The dimensionless distances between the walls which intersect the field lines are a_1 and a_3 for the poloidal and toroidal ducts, respectively. Here all lengths are normalized by L, half the distance between the pair of walls which are parallel (coplanar) to the field lines and are at $z = \pm 1$. To simplify the presentation of the analysis, we assume duct symmetry about the $z = 0$ plane, so only half the duct is treated, i.e., for $-1 \le z \le 0$. The walls are electrically conducting with uniform wall conductance ratio $c = \sigma_w t/\sigma$ where σ_w and σ are the electrical conductivities of the wall and the liquid metal, and t is the dimensionless wall thickness. The condition of equal conductance ratio for all walls is only to simplify the notation in our analytical presentation here. In fact the analysis and numerical modeling employed in this work allow for different values of c for different walls.

The ratio of the induced magnetic field produced by currents in the metal walls and in the liquid metal to the applied field is of order of $c^{1/2}R_m$ where

$$R_m = \mu\sigma U_o L,$$

is the magnetic Reynolds number, μ is the magnetic permeability of the liquid metal, and U_o is the coolant characteristic velocity. For a self-cooled blanket in a tokamak, $c^{1/2}R_m$ is at most of order of 10^{-2}; therefore, it is appropriate to neglect the induced field.

In addition, in a tokamak blanket the electromagnetic (EM) force is the dominant force determining the flow and pressure distributions throughout the liquid metal flow, except for thin boundary layers and interior layers. This is because the interaction parameter N, which represents the ratio of the EM force to inertial force, and the Hartmann number M, which represents the square root of the ratio of the EM force to viscous force, are typically of the order of 10^3-10^5 [1]. Here

$$N = \frac{\sigma B_o^2 L}{\rho U_o}$$

and

$$M = LB_o\left[\frac{\sigma}{\rho\upsilon}\right]^{1/2},$$

where ρ and υ are the fluid density and kinematic viscosity, respectively. The fact that $N \gg 1$ and $M \gg 1$ greatly simplifies the analysis since the inertial and viscous terms in the Navier-Stokes equation can be neglected except in thin boundary layers and interior layers where velocity gradients are large. There are two interior layers at the $x = x_o = a_1 \cos\theta_3 - a_3 \sin\theta_3$ and $x = 0$ cross sections. These interior layers separate the duct into three regions [4], region I for $x < x_o$, region II for $x_o < x < 0$, and region III for $x > 0$.

A.1 Governing Equations

The inertialess, inviscid, dimensionless equations governing the flow of a liquid metal in the core (outside the boundary or interior layers) of the flow are

$$\nabla p = \underset{\sim}{j} \times \hat{y} \tag{1a}$$

$$\underset{\sim}{j} = -\nabla\phi + \underset{\sim}{v} \times \hat{y} \tag{1b}$$

$$\nabla\cdot\underset{\sim}{v} = 0, \tag{1c}$$

$$\nabla\cdot\underset{\sim}{j} = 0. \tag{1d}$$

Here p, $\underset{\sim}{j}$, $\underset{\sim}{v}$, and ϕ are the pressure, electric current density, velocity, and electric potential normalized by $\sigma U_o B_o^2 L$, $\sigma U_o B_o$, U_o, and $U_o B_o L$, respectively.

In the core, the x, y, z velocity components u_c, v_c, w_c, and electric current density components j_{xc}, j_{yc}, j_{zc} are

$$u_c(x,y,z) = \frac{\partial \phi_c}{\partial z} - \frac{\partial p_c}{\partial x}, \tag{2a}$$

$$w_c(x,y,z) = -\frac{\partial \phi_c}{\partial x} - \frac{\partial p_c}{\partial z}, \tag{2b}$$

$$\int \frac{\partial v_c}{\partial y}(x,y,z)dy = -\int \left[\frac{\partial u_c}{\partial x} + \frac{\partial w_c}{\partial z}\right] dy, \tag{2c}$$

$$j_{xc}(x,y,z) = \frac{\partial p_c}{\partial z}, \tag{2d}$$

$$j_{zc}(x,y,z) = -\frac{\partial p_c}{\partial x}, \tag{2e}$$

$$j_{yc}(x,y,z) = -\frac{\partial \phi_c}{\partial y}, \tag{2f}$$

where $p_c(x,z)$ is the pressure, which is constant along magnetic field lines by virtue of Eq. (1a), and $\phi_c(x,y,z)$ is the electric potential in the core. The core potential varies linearly between the electric potential at the top wall, $\phi_t(x,z)$, and the electric potential at the bottom wall, $\phi_b(x,z)$,

$$\phi_c(x,y,z) = \phi_b(x,z) + \left[\phi_t(x,z) - \phi_b(x,z)\right]\left[\frac{y - y_b(x)}{y_t(x) - y_b(x)}\right], \tag{2g}$$

where $y_t(x) = x \tan \theta + a \sec \theta$, with $\theta = \theta_1$, $a = a_1$ for $x < x_o$, and $\theta = \theta_3$, $a = a_3$ for $x > x_o$, defines the coordinate of the top wall; and $y_b(x) = x \tan \theta$, with $\theta = \theta_1$ for $x < 0$ and $\theta = \theta_3$ for $x > 0$, defines the coordinate of the bottom wall.

The boundary conditions for the core variables have been derived by Shercliff [7]. At the top and bottom walls, the boundary condition for the core velocity is

$$\underset{\sim}{v}_c \cdot \hat{n} = 0. \tag{3a}$$

If the wall thickness $t \ll 1$, the boundary condition for the core current at the wall/fluid interface is

$$\underset{\sim}{j}_c \cdot \hat{n} = c\nabla^2 \phi_w \tag{3b}$$

where $\hat{n}$ is a unit vector normal to the wall into the liquid metal. The electric potential at the wall, ϕ_w, is uniform through its thickness neglecting $O(t^2)$ terms and ∇^2 is the two-dimensional Laplacian operator in the plane of the wall.

A.2 Reduced Governing Equations

The three-dimensional problem with many unknowns in the core (pressure, potential, three components of velocity and three components of current density) is completely solved once the solutions for $P_c(x,z)$, $\phi_t(x,z)$ and $\phi_b(x,z)$ are known. The equations governing these variables are provided by the boundary conditions (3a, b).

Integrating Eq. (2c) from y_b to y, we have

$$v_c(x,y,z) = v_c(x,y_b,z) + (y - y_b)\left[\frac{\partial^2 p_c}{\partial x^2} + \frac{\partial^2 p_c}{\partial z^2}\right] \tag{4}$$

Conditions (3a, b) applied at the bottom wall yields

$$v_c = u_c \tan \theta, \qquad \text{at } y = y_b \tag{5a}$$

$$\cos\theta\, j_{yc} - \sin\theta\, j_{xc} = c\left[\cos^2\theta\, \frac{\partial^2 \phi_b}{\partial x^2} + \frac{\partial^2 \phi_b}{\partial z^2}\right], \qquad \text{at } y = y_b \tag{5b}$$

where $\theta = \theta_1$ for $x < 0$ and $\theta = \theta_3$ for $x > 0$. The boundary conditions (3a, b) applied at the top wall yields

$$v_c = u_c \tan \theta, \qquad \text{at } y = y_t \tag{6a}$$

$$\sin\theta\, j_{xc} - \cos\theta\, j_{yc} = c\left[\cos^2\theta\, \frac{\partial^2 \phi_t}{\partial x^2} + \frac{\partial^2 \phi_t}{\partial z^2}\right] \qquad \text{at } y = y_t \tag{6b}$$

At the side wall ($z = -1$), condition (3b) gives

$$j_{zc} = c\left[\frac{\partial^2 \phi_s}{\partial x^2} + \frac{\partial^2 \phi_s}{\partial y^2}\right] \qquad \text{at } z = -1. \tag{7}$$

where $\phi_s(x,y)$ is the electric potential function at the side wall at $z = -1$.

Substituting the core equations into Eqs. (5-7), we arrive at the coupled partial differential equations governing P_c, ϕ_t, ϕ_b and ϕ_s. For regions I and III, the equations are

$$c\left[\cos^2\theta\,\frac{\partial^2\phi_t}{\partial x^2}+\frac{\partial^2\phi_t}{\partial z^2}\right]=\sin\theta\,\frac{\partial P_c}{\partial z}-\frac{\cos^2\theta}{a}(\phi_b-\phi_t), \tag{8a}$$

$$c\left[\cos^2\theta\,\frac{\partial^2\phi_b}{\partial x^2}+\frac{\partial^2\phi_b}{\partial z^2}\right]=-\sin\theta\,\frac{\partial P_c}{\partial z}+\frac{\cos^2\theta}{a}(\phi_b-\phi_t), \tag{8b}$$

$$c\left[\frac{\partial^2\phi_s}{\partial x^2}+\frac{\partial^2\phi_s}{\partial y^2}\right]=-\frac{\partial P_c}{\partial x}(x,-1), \tag{8c}$$

$$\frac{\partial^2 P_c}{\partial x^2}+\frac{\partial^2 P_c}{\partial z^2}=\frac{\sin\theta}{a}\left[\frac{\partial\phi_t}{\partial z}-\frac{\partial\phi_b}{\partial z}\right], \tag{8d}$$

where $\theta=\theta_1$, $a=a_1$ for region I, and $\theta=\theta_3$, $a=a_3$ for region III. In region II the corresponding equations are

$$c\left[\cos^2\theta_3\,\frac{\partial^2\phi_t}{\partial x^2}+\frac{\partial^2\phi_t}{\partial z^2}\right]=\sin\theta_3\,\frac{\partial P_c}{\partial z}-\sin\theta_3\cos^2\theta_3\,\frac{\phi_b-\phi_t}{x+a\sin\theta_3}, \tag{9a}$$

$$c\left[\sin^2\theta_3\,\frac{\partial^2\phi_b}{\partial x^2}+\frac{\partial^2\phi_b}{\partial z^2}\right]=\cos\theta_3\,\frac{\partial P_c}{\partial z}+\sin 2\theta_3\cos\theta_3\,\frac{\phi_b-\phi_t}{x+a\sin\theta_3}, \tag{9b}$$

$$c\left[\frac{\partial^2\phi_s}{\partial x^2}+\frac{\partial^2\phi_s}{\partial y^2}\right]=-\frac{\partial P_c}{\partial x}(x,-1), \tag{9c}$$

$$\frac{\partial}{\partial x}\left[(x+a\sin\theta_3)\,\frac{\partial P_c}{\partial x}\right]+\frac{\partial^2 P_c}{\partial z^2}=\sin^2\theta_3\,\frac{\partial\phi_t}{\partial z}+\cos^2\theta_3\,\frac{\partial\phi_b}{\partial z}. \tag{9d}$$

The boundary conditions necessary for solving the above set of coupled partial differential equations are provided by the prescribed flow conditions at upstream and downstream of the duct, the symmetry condition at $z = 0$, the continuities of electric potential and current density, and the conservation of total volumetric flow rate.

At $x = x_1$, upstream of the duct, and at $x = x_3$, downstream of the duct, the fully developed flow conditions are prescribed. The appropriate boundary conditions are

$$P_c = P_1 = \text{constant} \tag{10a}$$

$$\frac{\partial\phi_t}{\partial x}=\frac{\partial\phi_b}{\partial x}=\frac{\partial\phi_s}{\partial x}=0,\quad \text{at } x=x_1 \tag{10b,c,d}$$

and

$$P_c = P_2 = \text{constant} \tag{11a}$$

$$\frac{\partial\phi_t}{\partial x}=\frac{\partial\phi_b}{\partial x}=\frac{\partial\phi_s}{\partial x}=0\quad \text{at } x=x_3 \tag{11b,c,d}$$

The constants P_1 and P_2 ($P_1 > P_2$) are arbitrarily chosen. After the solution is found, every variable is multiplied by a scaling factor to get the desired volumetric flux such that

$$\int_{y_b}^{y_t}\int_{-1}^{0} u(x,y,z)\,dz\,dy = a_1$$

at every cross section.

At $z = 0$, the symmetry conditions apply

$$\frac{\partial P_c}{\partial z}=0, \tag{12a}$$

$$\phi_t=\phi_b=0\qquad \text{at } z=0 \tag{12b,c}$$

At each cross section, the continuities of electric potential and currents at the corners require that at $y = y_t$:

$$\phi_s(x,y_t) = \phi_t(x, -1), \tag{13a}$$

$$\cos\theta \frac{\partial\phi_s}{\partial y} - \sin\theta \frac{\partial\phi_s}{\partial x} = \frac{\partial\phi_t}{\partial z} \quad (x, -1) \tag{13b}$$

and at $y = y_b$:

$$\phi_s(x,y_b) = \phi_b(x, -1), \tag{13c}$$

$$\sin\theta \frac{\partial\phi_s}{\partial x} - \cos\theta \frac{\partial\phi_s}{\partial y} = \frac{\partial\phi_b}{\partial z} \quad (x, -1) \tag{13d}$$

where $\theta = \theta_1$ for region I, $\theta = \theta_3$ for region III; and for region II $\theta = \theta_1$ in condition (13b), while $\theta = \theta_3$ in condition (13d).

The velocity in the $O(M^{-1/2})$ thickness of the side layer (Fig. 1c) at $z = -1$ is $O(M^{n})$; thus the side layer carries an $O(1)$ volumetric flux (see, for example, Ref. 8 for a more detailed discussion of the side layer). The flow rate in the side layer is determined by the electric potential at the side wall and the electric potential in the core at $z = -1$:

$$\int_{s.l.} u\, dz = \phi_c(x,y,-1) - \phi_s(x,y) \tag{14}$$

where $\int_{s.l.}$ indicates integration across the side layer. Details of the side layer solution can be ignored provided that the total flow in the side layer plus the core remains constant at every cross section, namely

$$\frac{\partial}{\partial x}\int_{y_b}^{y_t}\left[\int_{s.l.} u\, dz + \int_{-1}^{0} u_c\, dz\right] dy = 0. \tag{15}$$

Condition (15) is necessary because the solutions for ϕ_t, ϕ_b, ϕ_s, and P_c completely determine $w_c(x,y,-1)$ which gives the flow into or out of the side layer.

Finally, the interior layers at $x = x_0$ and $x = 0$ do not carry any large $O(\delta)$ velocity or $O(1)$ electric current where δ is the layer thickness which is $O(M^{-1/2})$ if $N \gg M^{3/2}$ or $O(N^{-1/3})$ if $N \ll M^{3/2}$ [9]. Thus neglecting $O(\delta)$ terms, all core variables with the exception of v_c and w_c are continuous across these layers and currents along the walls are also continuous. The role of the interior layers is to match discontinuities in v_c and w_c between adjacent core regions.

The reduced coupled partial differential equations in ϕ_t, ϕ_b, ϕ_s, and P_c together with their boundary conditions are solved numerically using the finite difference method. The numerical scheme is similar to that presented in Ref. 8. Numerical solutions are obtained in all regions of the duct.

B. Backward Elbow

The coordinate system, the duct and magnetic field orientations are shown in Fig. 1b, here $\theta_3 < 0$ and $\theta_1 > 0$. The reduced governing equations in ϕ_t, ϕ_b, ϕ_s and P_c and their boundary conditions can be similarly derived and will not be repeated. In the backward elbow there is only one interior layer at $x = 0$. The lower part of the layer ($0 \le y \le a_1 \sec\theta_1$) separates the flow in region I and the lower part of region II, while the upper part of the layer separates the upper part of region II and region III. In the backward elbow, the value of $\partial P_c/\partial x$ is not continuous across the layer as is the case in the forward elbow, instead the integral of $\partial P_c/\partial x$ over y from bottom to top must be the same on both sides of the layer [10]. This can be obtained by integrating the conservation of mass equation over a z = constant section on both sides of the layer

$$a_1 \sec\theta_1 \frac{\partial P_c}{\partial x}(0^-,z)\Big|_I + a_3 \sec\theta_3 \frac{\partial P_c}{\partial x}(0^-,z)\Big|_{III} = (a_1 \sec\theta_1 + a_3 \sec\theta_3) \frac{\partial P_c}{\partial x}(0^+, z)\Big|_{II}. \tag{16}$$

A jump in $\partial P_c/\partial x$ implies a jump in u_c and an $O(\delta^{-1})$ v_c inside the layer, so there is an $O(1)$ volumetric flux flowing parallel to the magnetic field line inside the layer. The flow entering the layer from region I is split into two parts: one part enters region II, and the other part flows upward inside the interior layer then enters region III.

III. Results and Discussions

A joint ANL/KfK experiment to investigate MHD flows in both the forward and backward elbows will be conducted in 1991 at KfK. Some numerical results from the pretest analysis are presented in this section. The parameters of the test section are $a_1 = 2$, $a_3 = 1.33$, and $c = 0.057$. The experiment will include several orientations of the test section relative to the magnetic field lines. The main results presented here are for $\theta_3 = \pm 85°$ and fully developed flow conditions are imposed upstream and downstream in the analysis.

A. Forward Elbow

Figures 2a-e show the profiles of the velocity tangential to the top wall spanning from z = -1 to z = 1 at various distances from the elbow. The variable "s" is the dimensionless distance measured from the elbow along the wall, s < 0 indicates distance along the poloidal duct while s > 0 indicates distance along the toroidal duct. Initially at s = -2.44, the flow is fully developed, and velocity is uniform across z. (The fully developed boundary conditions were applied at s = -2.8. The results indicate that this location was sufficiently upstream for the flow to be fully developed.) As the flow approaches the elbow the three-dimensional effects cause the velocity to decrease near the center and increase near the sides (Fig. 2b, s = -0.14) which results in higher flow rate in the side layers. The velocity is markedly higher when the flow turns into the toroidal duct (Fig. 2c, s = 0.67), decreases gradually along the downstream direction (Fig. 2d, s = 9.94), and finally reaches the fully developed profile at s = 21.85 in Fig. 2e. Note that because of the smaller toroidal duct cross section, the fully developed velocity is higher than that in the poloidal duct.

Figures 3a-e show the profiles of the velocity tangential to the bottom wall. In these figures s = 0 is defined at the elbow of the bottom wall, and s = -3.44, -1.10, 1.72, 5.14, 17.21 in Figs. 3a,b,c,d,e, respectively. Because of the much weaker transverse component of the magnetic field in the toroidal duct, the flow becomes fully developed after a much longer distance than in the poloidal duct. Since the tangential velocity is never zero along the bottom wall or the top wall; and since velocity in the core at a cross section parallel to the field lines varies linearly between velocities at the bottom and top walls, results from Figs. 2 and 3 indicate that there is no region with stagnant fluid anywhere. This has positive heat transfer implications in tokamak blankets in which the bottom walls of the toroidal ducts constitute the blanket first walls where high surface heat depositions are expected. Stagnant pockets of coolant there would produce undesirable "hot spots."

Pressure drop, particularly the pressure drop due to the bend, is another important issue in the poloidal-toroidal flow geometry. Figure 4 shows the pressure variation along x at z = -1 and z = 0 (pressure is constant along magnetic field lines, i.e., in the y direction). In contrast to fully developed flow for which pressure is uniform across z and there are no axial currents, the pressure at the center is smaller than that at the side in the region where the flow is perturbed due to three-dimensional effects. The difference arises from the interaction between axial currents and the magnetic fields. Also shown in Fig. 4 is the reference pressure drop resulting from the upstream and downstream fully developed pressure gradients for $x < x_0/2$ and $x > x_0/2$, respectively. The pressure drop due to three-dimensional effects, ΔP_{3D}, is defined as the difference between the actual and reference pressure drops between two points far upstream and downstream:

$$\Delta P = \Delta P_{ref} + \Delta P_{3D}.$$

For ease of practical applications, we define

$$d_{3D} = \frac{\Delta P_{3D}}{\left.\frac{dp}{dx}\right|_{fd,pol}}$$

where $dp/dx|_{fd,pol}$ is the fully developed pressure gradient in the poloidal duct. Thus the pressure drop due to three-dimensional effects is equivalent to the fully developed pressure drop over an added dimensionless length d_{3D} in the poloidal duct. The results in Fig. 4 yield a value of 1.1 for d_{3D}. A parametric study was performed to provide analytical data for d_{3D} for various angles of θ_3, for conductance ratio ranges from 0.01 to 0.1 which are expected in tokamak blankets, and for various values of "a"(= a_1 = a_3). Results are presented in Fig. 5 for a = 2, θ_3 = 85° and 75°. Although the amount of three dimensional pressure drop varies with "a," d_{3D} was found to vary insignificantly among a = 2, 1, 0.5 for a given angle and conductance ratio as shown in Fig. 6. In general the additional pressure drop is of the order of the fully developed pressure drop over 1 characteristic length of the poloidal duct. This is relatively small compared to the overall pressure drop in the tokamak blanket, and should not be a concern in the design of the poloidal-toroidal coolant channels blanket.

B. Backward Elbow

Figures 7a-e show the profiles of the velocity tangential to the inner wall at various distances from the elbow. Far upstream (Fig. 7a, s = -3.0) and downstream (Fig. 7e, s = 13.8), the velocity is uniform across z. Negative values of velocity indicate reversed flow as is the case in Fig. 7c at s = 0.01. The fluid flows from the core in the toroidal duct into the interior layer parallel to the field lines at s = 0. In the forward elbow, the role of the interior layers is to match discontinuities in the transverse core velocities v_c and w_c, but the interior layer in the backward elbow carries a substantial fraction of the total flow rate. Part of the flow in region I completely bypasses region II, flows upward in the interior layer then enters region III. The amount of flow flowing within the

interior layer increases with increasing θ_3 and reaches a maximum when $\theta_3 = -45°$. As a result, there would be discontinuities in the axial core velocity across the layer. This is illustrated in Figs. 8a-e showing profiles of the velocity tangential to the outer wall. In these figures, s = 0 is defined at the elbow of the outer wall, the lower and upper parts of the interior layer intersect the wall at s = -1.51 and s = 17.2, respectively. The profiles along the wall in regions I and II just across the interior layer are given in Figs. 8a (s = -1.52) and 8b (s = -1.48); the abrupt decrease of velocity follows from the discontinuity in total flow rate. Similarly, Figs. 8d (s = 17.1) and 8e (s = 17.3) show the profiles just across the interior layer joining regions II and III, here the flow from the interior layer contributes to the abrupt increase in axial velocity. Near the elbow (s = 0.67, Fig. 8c) the flow is reversed and almost stagnant. However the stagnant flow is confined to only a small pocket around the elbow at the outer wall and would not be a concern. It can be easily eliminated by rounding the corner there.

The flow rate distributions through the interior layer, at far upstream and at downstream are presented in Fig. 9. The total dimensionless flow rate integrated over any cross section parallel to the field lines is 2. Note that there is a negative flow in the core of region III adjacent to the upper part of the interior layer. The velocity in the core there varies linearly between velocities at the bottom wall (Fig. 7c) and at the top wall (Fig. 8e). Since the velocity is more negative at the bottom wall, the net core flow when integrated over the cross section is negative.

The pressure drops due to three-dimensional effects, or equivalently d_{3D}, in the backward elbow were found to be similar qualitatively and quantitatively to those obtained for the forward elbow shown in Figs. 5 and 6.

Acknowledgments

This work was supported by the U. S. Department of Energy/Office of Fusion Energy under Contract W-31-109-ENG-38.

The authors acknowledge helpful discussions with Dr. Basil Picologlou of Argonne National Laboratory.

References

1. D. L. Smith et al., "Blanket Comparison and Selection Study," Fusion Technol. 8, 1 (1985).

2. S. Malang et al., "Self-Cooled Liquid-Metal Blanket Concept," Fusion Technol. 14, 1343 (1988).

3. J. C. R. Hunt and R. J. Holroyd, "Applications of Laboratory and Theoretical MHD Duct Flow Studies in Fusion Reactor Technology," Culham Laboratory Report CLM-R 169, Abingdon, Oxfordshire (1977).

4. T. J. Moon and J. S. Walker, "Liquid Metal Flow through a Sharp Elbow in the Plane of a Strong Magnetic Field," J. Fluid Mech. 213, 397 (1990).

5. T. J. Moon, T. Q. Hua, and J. S. Walker, "Liquid Metal Flow in a Backward Elbow in the Plane of a Strong Magnetic Field," accepted for publication in J. Fluid Mech.

6. C. B. Reed, B. F. Picologlou, and P. V. Dauzvardis, "Experimental Facility for Studying MHD Effects in Liquid Metal Cooled Blankets," Fusion Technol. 8, Part 2A, 257 (1985).

7. J. A. Shercliff, "The Flow of Conducting Fluids in Circular Pipes under Transverse Magnetic Fields," J. Fluid Mech. 1, 644 (1965).

8. T. Q. Hua, J. S. Walker, B. F. Picologlou, and C. B. Reed, "Three-Dimensional MHD Flows in Rectangular Ducts of Liquid-Metal-Cooled Blankets," Fusion Technol. 14, 1389 (1988).

9. J. C. R. Hunt and S. Leibovich, "Magnetohydrodynamic Flow in Channels of Variable Cross Section with Strong Transverse Magnetic Fields," J. Fluid Mech. 28, 241 (1967).

10. T. Q. Hua and B. F. Picologlou, "MHD Flow in a Manifold and Multiple Rectangular Coolant Duct of Self-Cooled Blankets," accepted for publication in Fusion Technol.

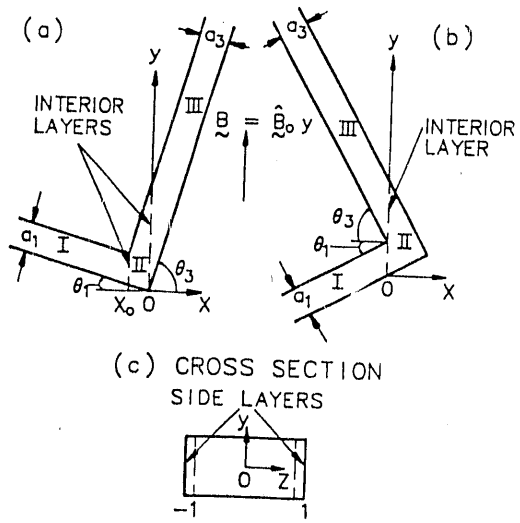

Figure 1. Schematics of the poloidal-toroidal duct cross sections (a) in the xy plane for the forward elbow, (b) in the xy plane for the backward elbow, and (c) in the yz plane of both elbows.

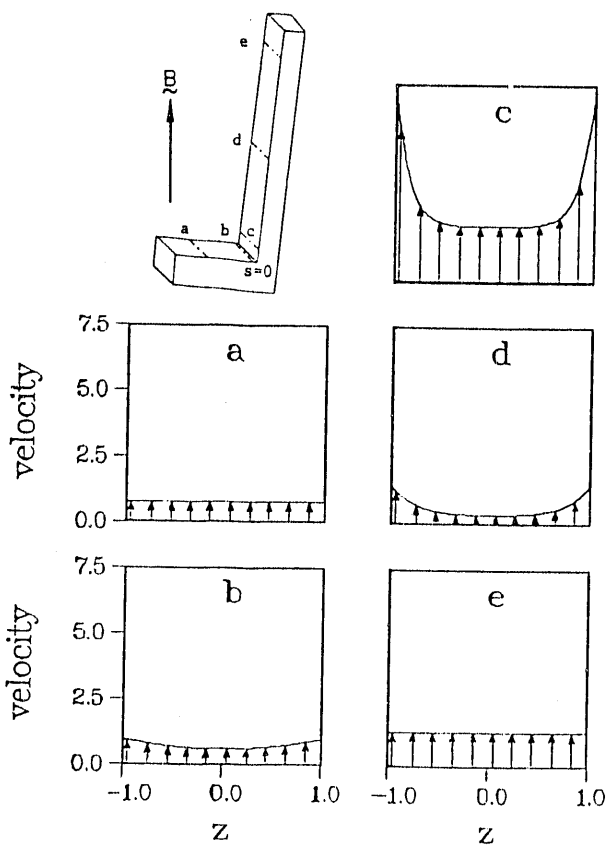

Figure 2. Profiles of velocity tangential to the top wall in the forward elbow from z = -1 to z = 1 at five different distances from the top wall elbow where s = 0 is defined, (a) s = -2.44, (b) s = -0.14, (c) s = 0.67, (d) s = 9.94, and (e) s = 21.85

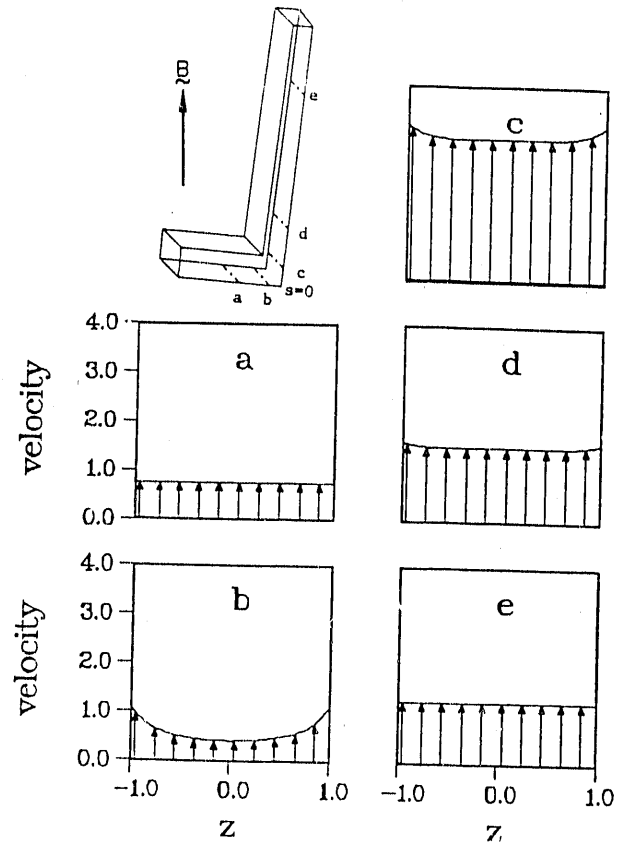

Figure 3. Profiles of velocity tangential to the bottom wall in the forward elbow from z = -1 to z = 1 at five different distances from the bottom wall elbow where s = 0 is defined, (a) s = -3.44, (b) s = 1.10, (c) s = 1.72, (d) s = 5.14, and (e) s = 17.21.

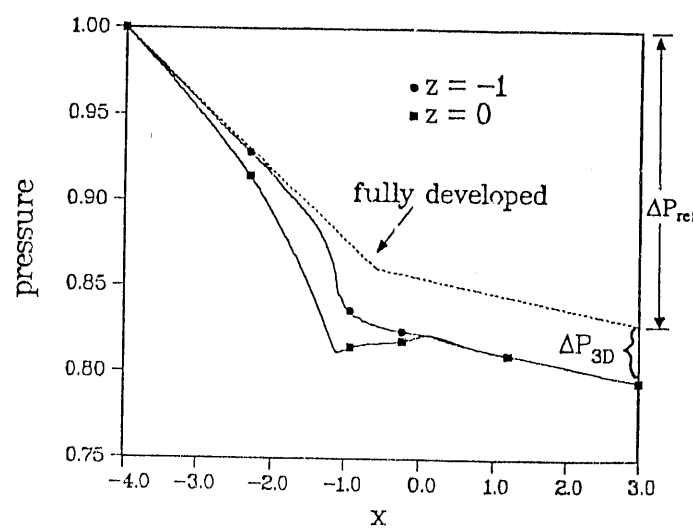

Figure 4. Pressure variation at z = -1 and z = 0. The reference pressure drop (dashed line) and three-dimensional pressure drop are also indicated.

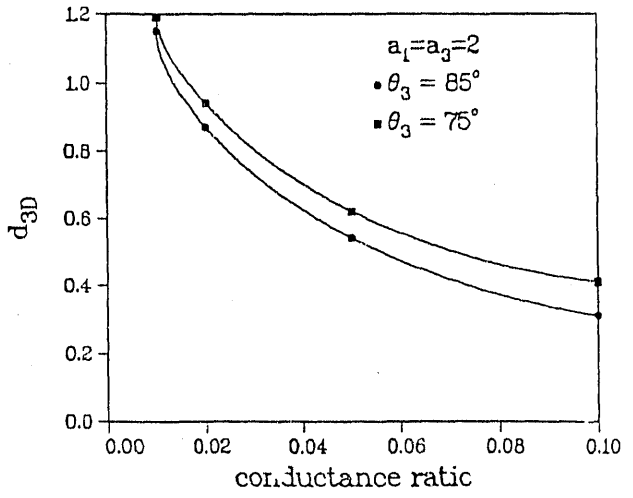

Figure 5. The three-dimensional pressure drops in the forward elbows expressed in terms of d_{3D} for $a_1 = a_3 = 2$.

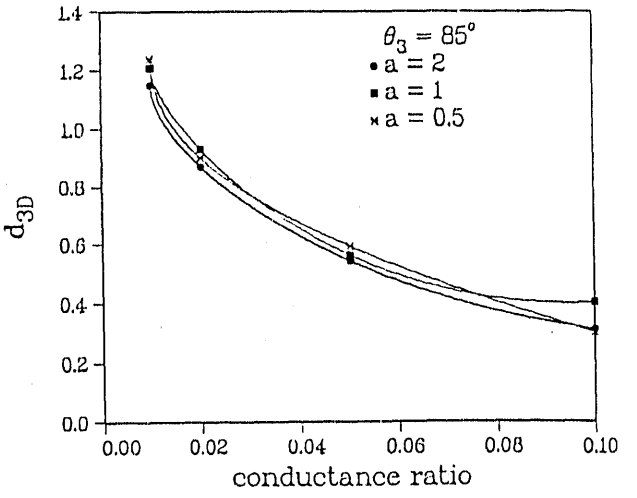

Figure 6. The three-dimensional pressure drops in the forward elbows expressed in terms of d_{3D} for $\theta_3 = 85°$.

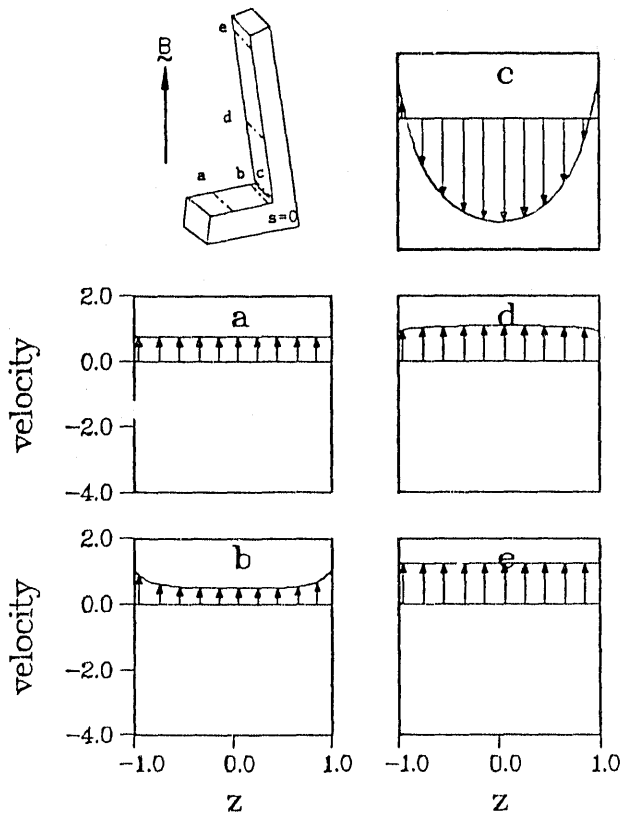

Figure 7. Profiles of velocity tangential to the inner wall in the backward elbow from z = -1 to z = 1 at five different distances from the inner wall elbow where s = 0 is defined, (a) s = -3.00, (b) s = -0.15, (c) s = 0.01, (d) s = 3.44, and s = 13.80.

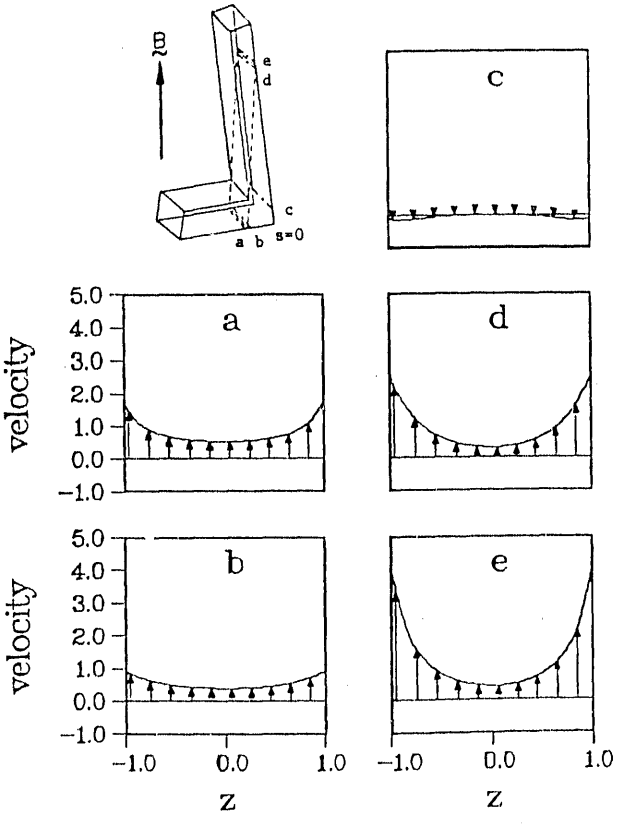

Figure 8. Profiles of velocity tangential to the outer wall in the backward elbow from z = -1 to z = 1 at five different distances from the outer wall elbow where s = 0 is defined, (a) s = -1.51, (b) s = -1.48, (c) s = 0.67, (d) s = 17.1, and (e) s = 17.3. The interior layer intersects the wall at s = -1.51 and s = 17.2.

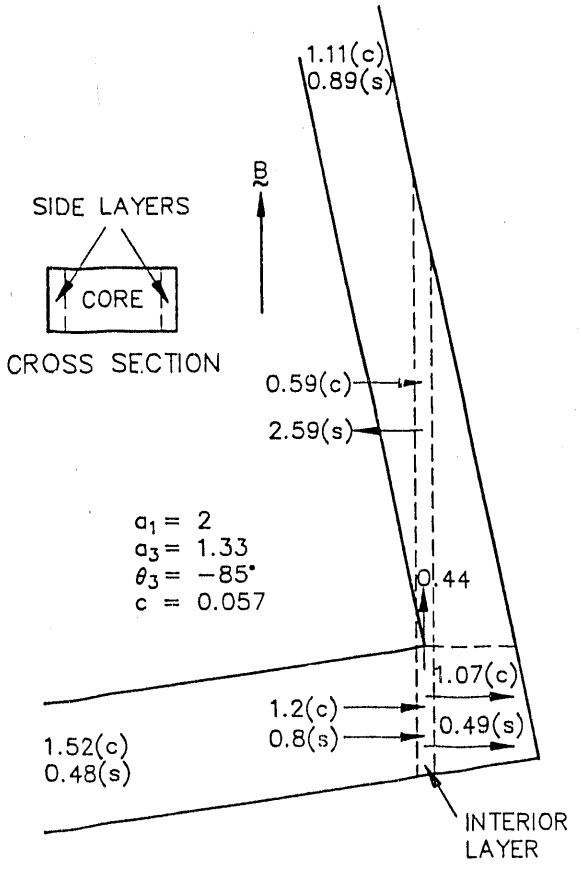

Figure 9. Flow rate distributions through the interior layer as well as in the core and the side layer in different regions of the backward elbow.

END

DATE FILMED

02 / 01 / 91